scientific reports

Check for updates

OPEN

# Strong anisotropic enhancement of photoluminescence in $WS_2$ integrated with plasmonic nanowire array

Chunrui Han[1,2]✉, Yu Wang[1], Weihu Zhou[1], Minpeng Liang[2] & Jianting Ye[2]✉

**Layered transition metal dichalcogenides (TMDCs) have shown great potential for a wide range of applications in photonics and optoelectronics. Nevertheless, valley decoherence severely randomizes its polarization which is important to a light emitter. Plasmonic metasurface with a unique way to manipulate the light-matter interaction may provide an effective and practical solution. Here by integrating TMDCs with plasmonic nanowire arrays, we demonstrate strong anisotropic enhancement of the excitonic emission at different spectral positions. For the indirect bandgap transition in bilayer $WS_2$, multifold enhancement can be achieved with the photoluminescence (PL) polarization either perpendicular or parallel to the long axis of nanowires, which arises from the coupling of $WS_2$ with localized or guided plasmon modes, respectively. Moreover, PL of high linearity is obtained in the direct bandgap transition benefiting from, in addition to the plasmonic enhancement, the directional diffraction scattering of nanowire arrays. Our method with enhanced PL intensity contrasts to the conventional form-birefringence based on the aspect ratio of nanowire arrays where the intensity loss is remarkable. Our results provide a prototypical plasmon-exciton hybrid system for anisotropic enhancement of the PL at the nanoscale, enabling simultaneous control of the intensity, polarization and wavelength toward practical ultrathin photonic devices based on TMDCs.**

Two-dimensional semiconducting transition metal dichalcogenides (TMDCs) have recently attracted considerable interest because of tunable bandgap, tightly bound excitons, and highly tunable excitonic properties[1], enabling applications in various photonic and optoelectronic devices ranging from infrared to visible spectra, such as light-emitting diodes[2–4], photodetectors[5,6], photovoltaics[7], modulators[8,9], nanoscale quantum devices[10–12], etc. To be a light emitter, an important property is a linear polarization, which is highlighted in areas like ultrasensitive sensing, super-resolution imaging, medical diagnosis, and optical communications[13–20]. PL of TMDCs is intrinsically linearly polarized under linear excitation, because of the coherent superposition of excitonic states in $+/-K$ valleys at the corners of Brillouin zones. However, due to the Coulomb exchange interaction and intervalley scattering, valley coherence is severely suppressed at room temperature, resulting in random polarization in practice. To recover the valley coherence, resonant nanocavities have been proposed to either generate exciton–polariton quasiparticles[21,22] or accelerate the electron–hole recombination rate to surpass quantum decoherence[12]. Despite these efforts, it remains difficult to achieve a strong PL signal with high linearity and conventional polarizers that are bulky and of high losses are still in use. To be compatible with on-chip integration, new types of anisotropic modulation of the excitonic emission are highly demanding.

Optical processes such as absorption and emission in quantum emitters can be greatly modified by using optical cavities because the interaction between light and matter closely depends on the local density of electromagnetic modes[23,24]. The enhancement occurs when the interaction between EM modes and emitters overcomes the damping in the system, such as $MoS_2/WS_2$ with nanodisks, dimer nanoantennas, and bull's eye-shaped Bragg reflectors due to Purcell effect[25–28], and Fano resonance in the hybrid of $MoS_2$-bowtie nanoantenna array[29]. To further emphasize the optical anisotropy, metallic nanowires are more advantageous, which enable tailoring multiple parameters of light emission in a single device, e.g. wavelength, polarization, phase, and direction[30–37]. Regarding the polarization, the anisotropy arises from generally the form-birefringent effect of subwavelength nanowire arrays, which is characterized as a reflection of the TE polarization and the transmission of the TM polarization

[1]Institute of Microelectronics, Chinese Academy of Sciences, Beijing 100029, China. [2]Device Physics of Complex Materials, Zernike Institute for Advanced Materials, University of Groningen, Nijenborgh 4, 9747 AG Groningen, The Netherlands. ✉email: hanchunrui@ime.ac.cn; j.ye@rug.nl

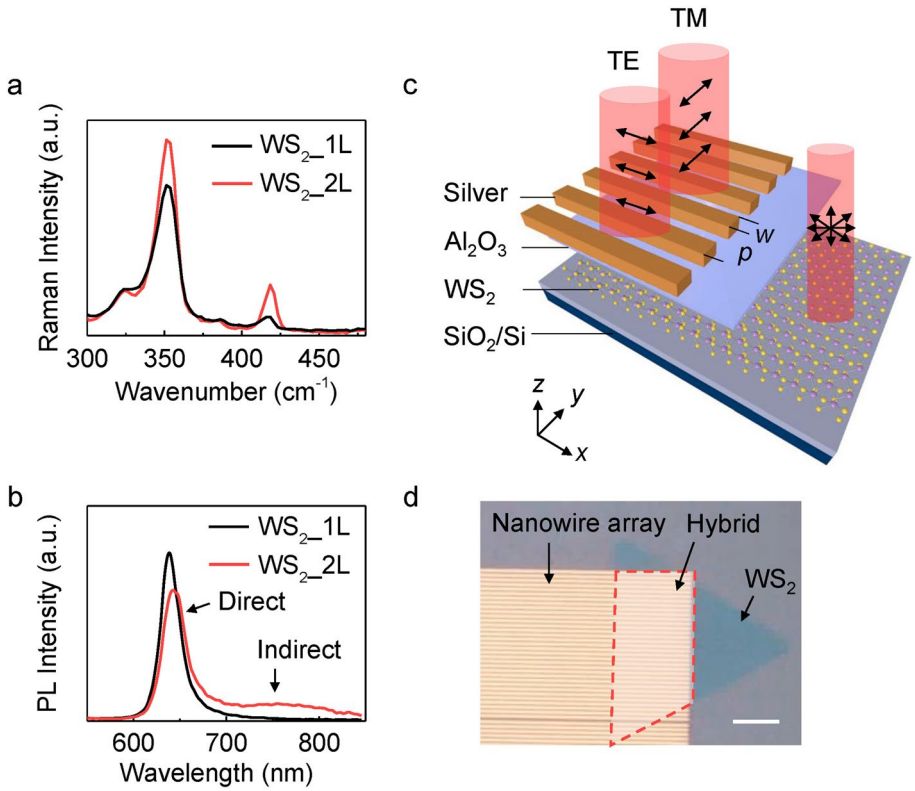


**Figure 1.** Device configuration of the $WS_2$-Ag wire array hybrid nanostructure. (**a**) Raman spectra of mono- and bilayer $WS_2$. (**b**) PL spectra of mono- and bilayer $WS_2$. (**c**) 3D schematic view of the hybrid device consisting of silver nanowire array on top of $WS_2$ separated by a thin layer of $Al_2O_3$. (**d**) Optical microscopy image of the $WS_2$-Ag wire hybrid nanostructure. The scale bar is 6 μm.

and determined by the aspect ratio of a nanowire[38,39]. Whereas, intriguing processes of plasmonic resonance and coherent interference that could also lead to strong anisotropy have not been properly treated. Hence, the radiative behaviors of a wire array-TMDCs hybrid system certainly deserve to be investigated comprehensively.

Here, we demonstrate strong anisotropic enhancement of the PL in a plasmon-exciton hybrid system consisting of a plasmonic nanowire array and $WS_2$. For the indirect bandgap transition around 750 nm, up to 7 (4.2) folds enhancement was achieved with the PL polarization perpendicular (parallel) to the long axis of the nanowire. The enhancement arises from the Purcell effect which is attributed to the coupling of $WS_2$ with localized (guided) surface plasmon modes in nanowire arrays of different periods. Although we observed enhancement for both TE and TM polarizations, the magnitudes of the enhancement are different, leading to a high degree of linearity. For the direct bandgap transition, a high degree of linearity was also observed because of the enhancement/suppression of the PL in TE/TM polarization directions, *i.e.* plasmon-enhanced coherent scattering of the TE polarization in the forward direction and the high reflection of the TM polarization in the backward direction. The degree of the linearity is found to depend on the wire width and period of the array while it is less influenced by the polarization of the excitation laser. Our results demonstrate the unique anisotropic light-matter interactions in a highly confined TMDC-metasurface device, which offer the possibility of manipulating the intensity, polarization, and wavelength of the scattered light in one single device and provide guidelines for establishing the ultrathin optical devices with multi-functionalities.

## Results

**Device configuration.** $WS_2$ flakes were grown by chemical vapor deposition on silicon wafers with thermally grown $SiO_2$ of 285 nm (Supplementary note 1). The crystal is identified by the $E'$ ($E^1_{2g}$) and $A'_1(A_{1g})$ Raman bands around 350 and 418 $cm^{-1}$ (Fig. 1a and Figure S1) for mono- (bi-) layer, respectively[40]. The layer numbers are characterized through the PL spectra, in which only the direct bandgap transition around 636 nm can be observed in the monolayer $WS_2$ (black curve in Fig. 1b) while an additional broad emission appears around 750 nm (1.65 eV) corresponding to the indirect bandgap transition of a bilayer $WS_2$ (red curve in Fig. 1b)[41,42]. For the bilayer $WS_2$ grown by chemical vapor deposition, the intensity of the PL at 640 nm is as strong as that of the monolayer. This is probably due to the partial coverage of the second layer, leaving a mixture of monolayer and bilayer (Supplementary note 5). To establish a practical device, a 20 nm thick $Al_2O_3$ layer was deposited to protect the $WS_2$ from dopants in the ambient atmosphere. Nanowire arrays with varying period $p$ and wire width $w$ were fabricated subsequently on top using electron-beam lithography followed by silver metallization

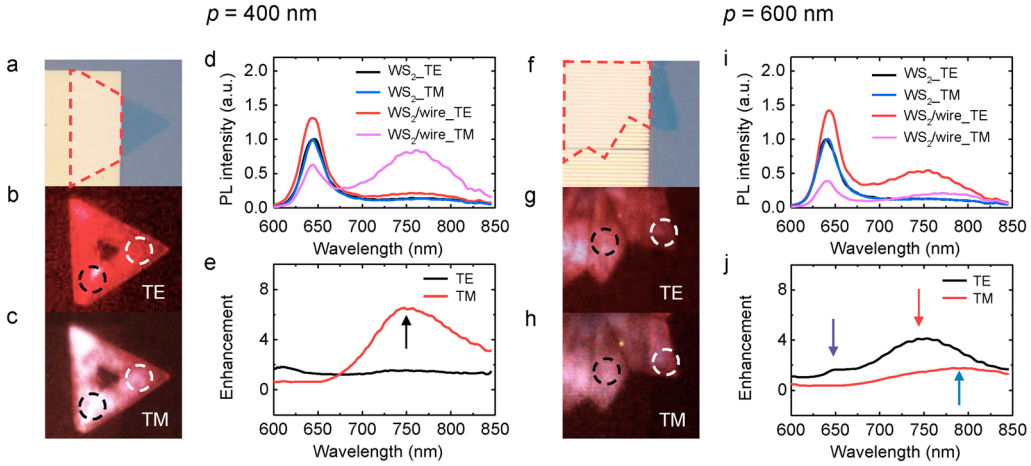


**Figure 2.** Anisotropic enhancement of the PL emission in $WS_2$-Ag wire hybrid nanostructures. (**a**) Optical image of the hybrid nanostructure. $WS_2$ covered by the nanowire array ($p = 400$ nm, $w = 140$ nm) is enclosed by the red dashed lines. (**b**)–(**c**) The corresponding PL images for TE and TM polarizations. The dashed circles indicate the positions of the spectral measurement. (**d**) Normalized PL spectra of the $WS_2$ bilayer with (red and pink curves) and without (black and blue curves) silver nanowire array for TE and TM polarizations respectively. (**e**) PL enhancements of the hybrid nanostructure relative to the pristine $WS_2$ for TE (black curve) and TM (red curve) polarizations, respectively. (**f**)–(**j**) The corresponding results for the hybrid nanostructure with $p = 600$ nm and $w = 300$ nm.

(Fig. 1c). $WS_2$ flakes are partially covered by the nanowire array to define regions with and without photonic structures for comparison, where the $WS_2$-Ag hybrid region is indicated by a red dashed box (Fig. 1d).

**Anisotropic enhancement behaviors of the PL in the direct and indirect bandgap transitions.** *Experimental characterization of the anisotropic enhancement.* After patterning nanowire arrays, the hybrid devices were firstly characterized by polarization-resolved PL imaging (Supplementary note 2). Briefly, samples were excited by a 450 nm light-emitting diode and the polarization of the PL emission was resolved by rotating a polarizer before the CCD camera. For the $p = 400$ nm wire array, the optical image is shown in Fig. 2a where a triangular-shaped $WS_2$ (blue region) is partly covered by the metasurface (yellow region). PL images of the TE and TM polarized light are shown in Fig. 2b,c, respectively. The region covered by the array is slightly brighter than that of the pristine $WS_2$ for TE (Fig. 2b) but significantly brighter for TM (Fig. 2c). Note that the CCD camera showed slightly anisotropic responses between TE and TM polarizations, therefore one should NOT compare the color (i.e. intensity) between TE and TM images. Nevertheless, within each polarization image, one can roughly evaluate the enhancement of the PL intensity.

To quantify the enhancement, polarization-resolved PL spectra were taken in regions of pristine $WS_2$ and hybrid $WS_2$-Ag wire array respectively (Supplementary note 3). The samples were excited by a 532 nm laser with the incident polarization fixed in the TE direction. The PL emission was collected in the TE and TM directions by rotating the analyzer to be parallel and perpendicular to the long axis of the nanowire, respectively. PL spectra of the pristine bilayer $WS_2$ are shown by the black and blue curves in Fig. 2d. The coincidence between TE and TM implies that the PL emission is almost randomly polarized due to the valley depolarization mechanism, such as Coulomb exchange interaction and intervalley scattering at room temperature[43]. A drastic change between TE and TM is observed when the nanowire array is fabricated on top as shown by the red and pink curves in Fig. 2d. For the direct bandgap transition around 640 nm, the PL intensity is 1.3/0.6 times enhanced for TE/TM, respectively (Fig. 2d). In contrast, for the indirect bandgap transition around 750 nm, both TE and TM are amplified. Specifically, the enhancement of the PL relative to the pristine $WS_2$ is 7 for TM and 1.5 for TE as shown by the red and black curves in Fig. 2e. The enhancements are different at different spectral positions, implying that the underlying mechanisms involving the plasmon-mediated excitonic emission are different at different optical bandgap transitions.

For $p = 600$ nm wire arrays, the optical image of the $WS_2$-Ag wire hybrid nanostructure is shown in Fig. 2f. The region covered by the nanowire array is brighter than that of the pristine $WS_2$ in the TE polarized image (Fig. 2g) whereas it becomes significantly darker for the TM polarized image (Fig. 2h). The color contrast between the regions with and without the metasurface can be further verified by the PL spectral measurement. For the TE polarized emission, the intensity relative to that of the pristine $WS_2$ is 1.4 and 4.2 times enhanced for the direct and indirect bandgap transitions (the purple and red arrows in Fig. 2j), consistent with the brighter color in Fig. 2g. In contrast, for the TM polarized emission, the intensity of the PL in the hybrid region is only 39% of the pristine $WS_2$ for the direct bandgap transition (pink curve in Fig. 2i), resulting in the darker PL image as shown in Fig. 2h. The larger suppression of the TM polarization leads to the larger anisotropy between TE and TM for the 600 nm period wire array than that of the 400 nm (red and pink curves in Fig. 2d,i). For the indirect bandgap transition, the PL is greatly enhanced in the TE polarization direction, which is perpendicular to that

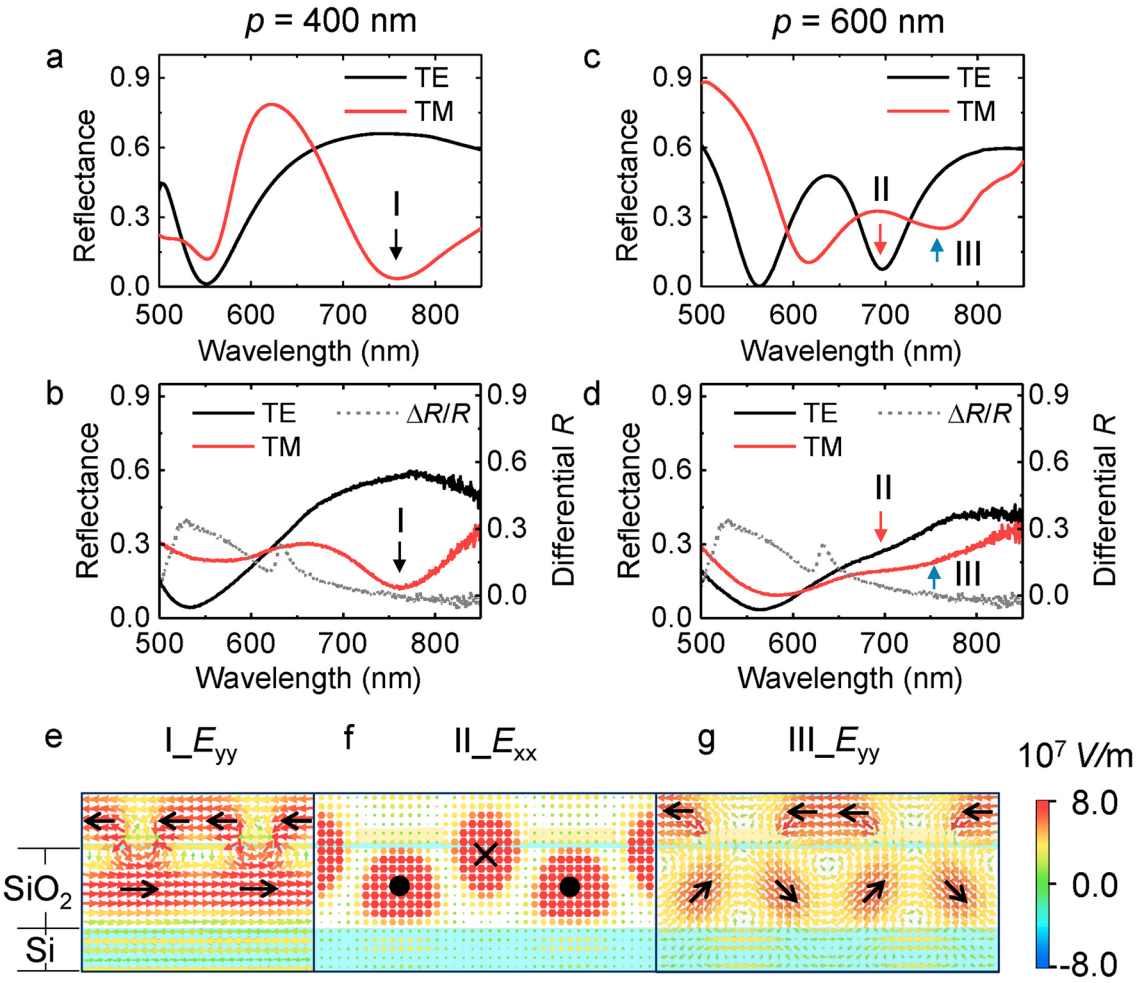


**Figure 3.** Polarization resolved white light spectra. (**a**)–(**b**) Reflectance spectra of the $WS_2$-Ag wire hybrid nanostructure with $p = 400$ nm in simulation (**a**) and experiment (**b**) for TE and TM polarizations, respectively. (**c**)–(**d**) The corresponding results for the hybrid nanostructure with the period of the nanowire array 600 nm. Differential reflectance peaks ~ 630 nm [dashed grey curves in (**b**) and (**d**)] indicate the absorption of the $WS_2$ monolayer. (**e**)–(**g**) Distributions of the electric fields at the $x = 0$ nm cutting plane for resonance modes I-III respectively. Black arrows indicate the directions of electric dipoles.

observed in the 400 nm period wire array, implying that the period of the nanowire array is essential to control the direction of the polarization.

We'd like to emphasize that with significant improvement in polarization, the total intensity of the emission does not decay but increases due to the energy transfer. This is in contrast to the conventional passive birefringent crystal, through which the light of TE polarization is much more blocked than TM polarization thus the total intensity keeps descending due to the scattering and absorption of the crystal. In this regard, our nanowire array is NOT just a simple polarizer.

*The mechanism for anisotropic enhancement of the indirect bandgap transition.* To understand the anisotropic enhancement behaviors observed above, optical responses of the nanowire arrays are simulated by a commercial finite-difference time-domain algorithm (FDTD Solution, Lumerical) for $x$ and $y$ polarization incidences. For the array of $p = 400$ nm, $w = 140$ nm, we find a pronounced reflectance dip around 750 nm (mode I) for the TM polarization as indicated by the black arrow in Fig. 3a, which is consistent with the experimental results shown in Fig. 3b. This dip overlaps well with the indirect bandgap transition, hence could be the main reason for significant PL enhancement (7x) in the TM polarization direction (black arrow in Fig. 2e). The dip is intrinsically a localized surface plasmon mode whose electric fields are densely localized around the edge of nanowires (Fig. 3e) exhibiting strongly enhanced fields and a high local density of states. The coupling of excitons with the confined plasmonic fields accelerates the decay rate of the spontaneous emission, causing a brighter PL image in the 400 nm period nanowire array (Fig. 2c). Moreover, the driving field is oscillating in the TM direction, thereby polarizing the PL emission in the same direction.

For $p = 600$ nm wire arrays, we find a reflectance dip around 700 nm (mode II) for the TE polarized light in both numerical simulation and experiment (red arrows in Fig. 3c,d). Its electric field distribution (Fig. 3f)

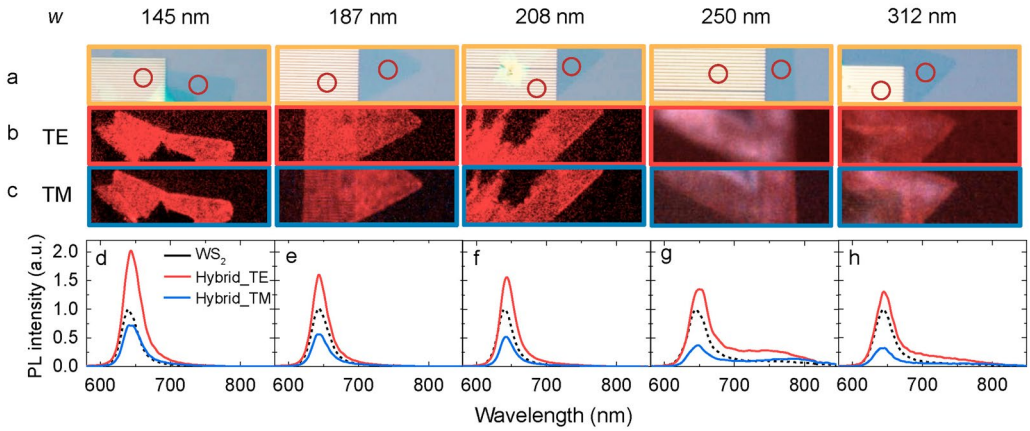


**Figure 4.** Anisotropic enhancement of the direct bandgap emission as a function of the wire width. (**a**) Optical images of the $WS_2$-Ag wire hybrid nanostructures. From left to right, the width of the nanowire is 145, 187, 208, 250 and 312 nm, respectively. (**b**)–(**c**) Corresponding PL images for TE and TM polarizations. (**d**)–(**h**) Corresponding PL spectra for the pristine $WS_2$ (black dashed curves), $WS_2$-Ag wire hybrid nanostructures in TE (red solid curves) and TM (blue solid curves) polarization directions.

indicates the energy is mainly concentrated in dielectric layers. The fields are polarized along the wire with opposite phases in a unit cell, resulting in a pronounced magnetic resonance around indirect excitons that accounts for the 4.2 folds enhancement of the PL emission in the TE polarization direction (red arrow in Fig. 2j). We identify mode II as a plasmonic waveguide mode rather than a localized surface plasmon of individual wire[44], because the electromagnetic fields are confined in dielectric layers between the top metal and the bottom silicon instead of metal surfaces whose distributions follow closely the period of the wire array. Compared to mode I, the loss of this mode is smaller because of vanishing dissipation from the displacement currents of the metal due to the opposite phases of electric dipolar resonances in the dielectric layer. However, the mode volume is larger, therefore the enhancement is slightly weaker (4.2x) compared with mode I (7x). For the TM polarization, a reflectance dip appears around 750 nm (blue arrows in Fig. 3c,d) which is indicative of a resonance mode III, providing the driving force for the enhancement of the TM polarized emission (the blue arrow in Fig. 2j). The electric dipolar resonance on the top surface of wire arrays is quite similar to that of mode I, but the magnitude is only 1/4 (Fig. 3g), hence the enhancement of the PL emission is relatively small (1.8x).

Combining the experimental and simulation results, we can now understand the strong anisotropic enhancement of the indirect bandgap transition achieved in the bilayer $WS_2$-silver nanowire hybrid nanostructure. The enhancement is attributed to the coupling of excitons with the plasmonic modes of the nanowire array through which the spontaneous emission rate, as well as the quantum yield, is greatly boosted in the bilayer $WS_2$. The degree of the enhancement depends on the intensity of local fields, the mode volume, and the system loss. Among the three modes, mode I is a localized plasmon mode with maximum field intensity and minimum mode volume, hence it enables the largest PL enhancement (7x). Mode II is a plasmonic waveguide mode whose mode volume is much larger than that of mode I but the loss is smaller due to the magnetic resonance, hence the PL enhancement remains large (4.2x). Mode III belongs to a plasmonic mode whose field distribution is similar to that of mode I but the intensity of the local field is much weaker. In addition, the mode volume is larger because of the larger period, therefore leading to the smallest PL enhancement (1.8x). The polarization direction of the enhancement is consistent with the oscillation direction of the electric dipolar resonance in the nanowire array which can be either parallel (mode II) or perpendicular (mode I and III) to the nanowires.

*The mechanism for anisotropic enhancement of the direct bandgap transition.* As indicated by the experimental results in Fig. 2d,i, the anisotropy for the direct bandgap transition is due to the enhancement of the PL in the TE polarization direction and the suppression of the PL in the TM polarization direction (Fig. 2d,i). However, as demonstrated in this section, the TE enhancement cannot be accounted for *only* by the plasmonic effect. Rather, the interference of the periodic nanowire array plays an important role.

Before discussing the mechanism, we'd like to confirm the robustness of the experimental observation by varying the wire width while fixing the array period at 600 nm (optical images in Fig. 4a). PL images indicate that the $WS_2$-wire hybrid region is brighter in the TE polarization direction (Fig. 4b) and darker in the TM polarization direction (Fig. 4c). Moreover, with increasing the wire width from 145, 187, 208, 250 to 312 nm, the degree of the enhancement relative to the pristine $WS_2$ (dashed black curve in Fig. 4d–h) decreases from 2.0/0.72, 1.6/0.56, 1.56/0.52, 1.35/0.37 to 1.30/0.32 for the TE/TM polarized light (red/blue curves in Fig. 4d–h), implying that the wire width is an effective parameter in tailoring the intensity and anisotropy of the PL emission: while narrower wires are more efficient to enhance the PL along the wire, wider wires are more suitable to suppress the PL in perpendicular to the long axis of the wire.

Now we turn to numerical simulations where the dielectric substrates ($Al_2O_3$, $SiO_2$ and silicon layers) are added in a step-by-step fashion. To substantiate the experiment in Fig. 4, we choose nanowire arrays with

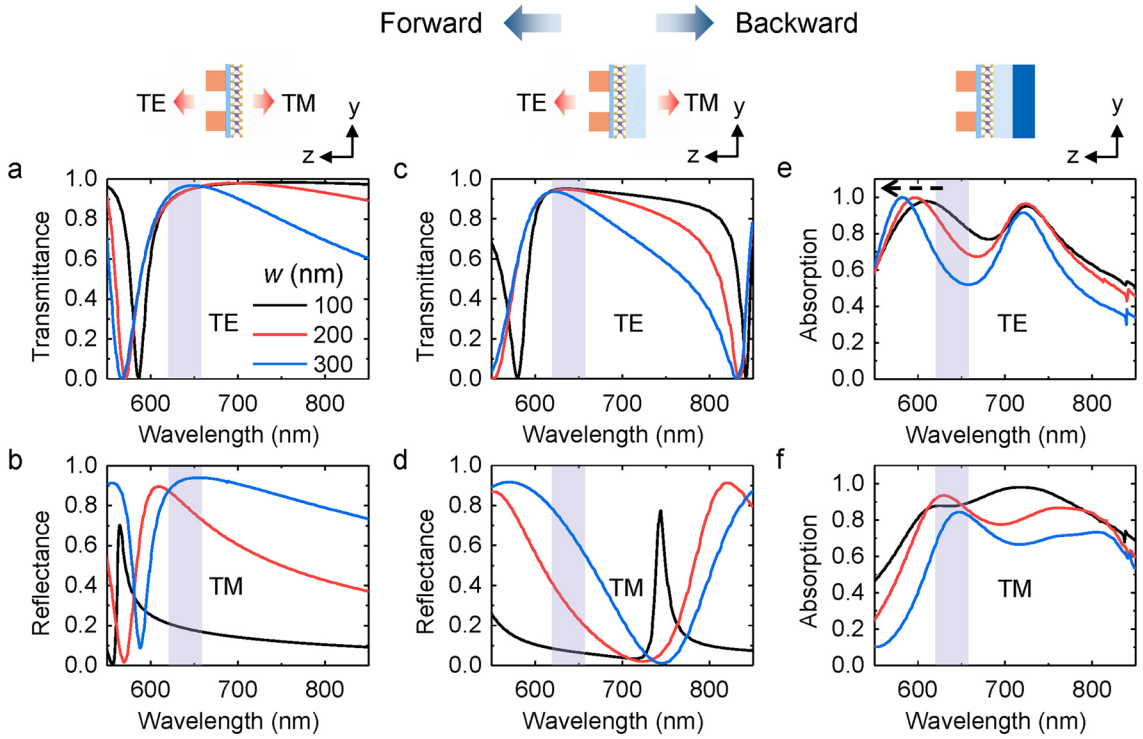


**Figure 5.** Polarization resolved spectra as a function of the wire width by simulations. (**a**)–(**b**) Transmittance of the TE polarized light and reflectance of the TM polarized light under the forward incidence for the nanowire array on $Al_2O_3$ substrate with $p = 600$ nm, $w = 100$, 200, 300 nm respectively. (**c**)–(**d**) The corresponding spectra of the nanowire array on $Al_2O_3/SiO_2$ substrate. (**e**)–(**f**) Absorption spectra of the TE and TM polarized light under the backward incidence for the nanowire array on $Al_2O_3/SiO_2/Si$ substrates.

$p = 600$ nm, $w = 100$, 200 and 300 nm in Fig. 5. For the forward incidence, that is, the light propagates at the positive z-direction, the transmittance of the TE polarized light around the wavelength of the direct bandgap transition (marked by the purple strips in Fig. 5) is high as shown in Fig. 5a,c for the nanowire array on $Al_2O_3$ and $Al_2O_3/SiO_2$ respectively. Moreover, the reflectance of the TM polarized light increases step by step with the wire width, denoted by the black, red, blue curves as shown in Fig. 5b and d. It suggests that the nanowire array allows high transmission of the TE polarized PL in the forward direction and a tunable reflection of the TM polarized PL in the backward direction, consistent with the near field distributions of the nanowire array in $E_{xx}$ and $E_{yy}$ directions (Figure S2).

To be detailed, in Fig. 5e, absorption spectra of the nanowire array on $Al_2O_3/SiO_2/Si$ substrates indicate that plasmonic resonances appear around 600 nm. These peaks locate on the blue side of the spectral wavelength of the direct bandgap transition, offer feasible excitation and energy transfer between nanowires and $WS_2$ excitons, leading to the enhancement of the PL emission in the TE polarization direction[45,46]. With increasing the wire width, the peak shifts to the shorter wavelength as indicated by the dashed black arrow in Fig. 5e, hence the spectral overlap between plasmons and excitons decreases, resulting in the descending trend of the PL enhancement in the TE polarization direction as indicated by the red curves in Fig. 4d–h. For the TM polarization, broadband absorption of plasmonic resonance appears around the direct bandgap transition (Fig. 5f) which is possible to accelerate the spontaneous emission rate. However, the emission in the TM polarization is mainly reflected by the nanowire array and the reflection increases with the wire width, resulting in the suppression of the PL in the forward direction and the descending trend of the PL intensity with the wire width (blue curves in Fig. 4d–h).

However, note that in Fig. 5e the direct band emission does not coincide with the plasmonic resonance in TE polarization. Especially for $w = 300$ nm, the emission approaches the valley of the absorption spectra, calling for an alternative mechanism to explain the TE enhancement. Since the nanowire array resembles a diffraction grating, the inevitable result is the constructive interference at the angle $\theta$ with $p\sin\theta = m\lambda$, where $\theta$ is the angle between the grating surface and the emission direction of light, $p$ is the period of the grating and $\lambda$ is the emission wavelength[47]. Light collected in the normal direction corresponds to $\theta = 90°$ which is an interference maximum, thus the emission in the TE polarization is enhanced as shown in Fig. 4b.

As a result, the strong anisotropy of the direct bandgap transition is attributed to the zeroth-order constructive interference of the nanowire array in addition to the active plasmonic resonance on the blue side of the emission wavelength in the TE polarization direction as well as the tunable reflectance of the nanowire array in the TM polarization direction.

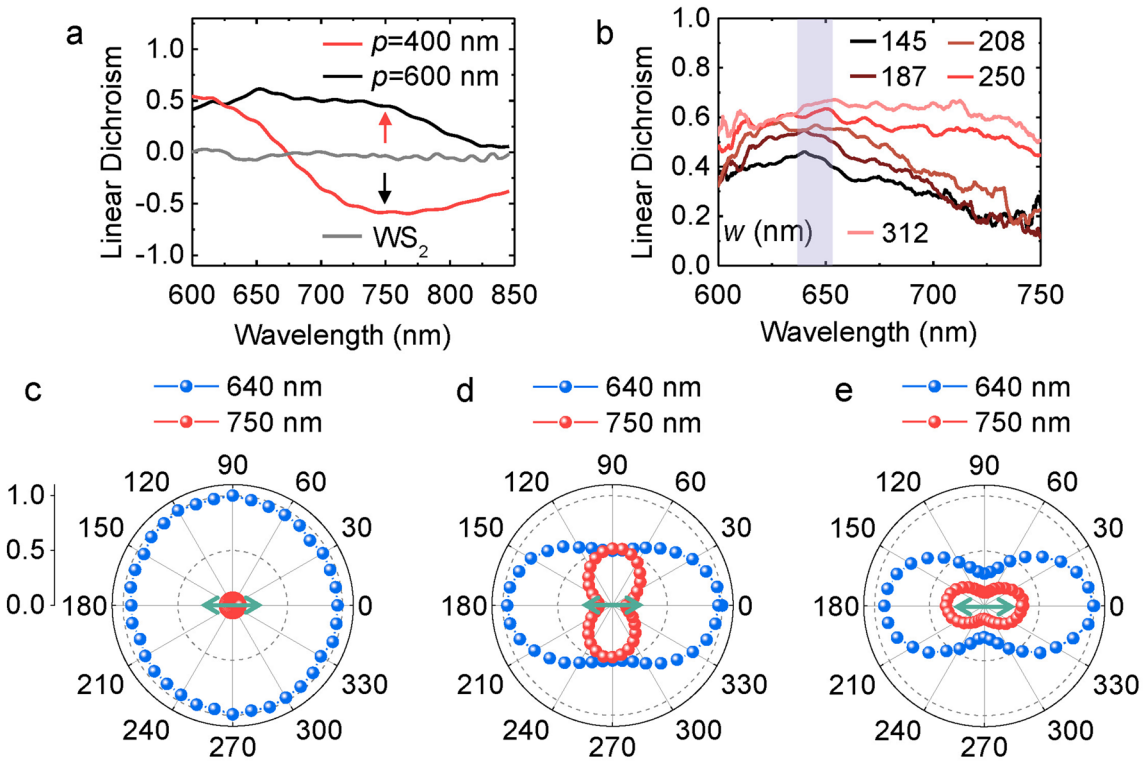


**Figure 6.** Linearity of the direct and indirect bandgap transitions modulated by the plasmonic nanowire array. (**a**) Linear dichroism of the PL emission for pristine bilayer $WS_2$ (grey curve) and $WS_2$-Ag hybrid nanostructures with $p = 400$ (red curve) and 600 nm (black curve) respectively. (**b**) Linear dichroism of $WS_2$-Ag hybrid nanostructure with $p = 600$ nm as a function of the wire width. (**c**)–(**e**) Normalized PL peak intensity as a function of the detection angle for pristine bilayer $WS_2$ (**c**) and hybrid nanostructures with $p = 400$ (**d**) and 600 nm (**e**), respectively. Blue/red dots indicate the emission of direct/indirect bandgap transitions, respectively. Here, zero corresponds to the center and 1.0 to the outermost dashed circle. Green arrows indicate the long axis of the nanowire.

*Polarization modulation through the anisotropic enhancement of the PL.* To quantify the PL anisotropy as a function of the period and wire width, linear dichroism (LD) calculated as $LD = (I_{TE} - I_{TM})/(I_{TE} + I_{TM})$ is shown in Fig. 6. For the indirect bandgap transition, in contrast to the diminishing LD in pristine $WS_2$, a positive LD of 0.5 is achieved in the nanowire array with $p = 600$ nm, $w = 300$ nm for the indirect bandgap transition (red arrow in Fig. 6a). Additionally, a large negative LD ~ −0.6 is observed for the nanowire array with $p = 400$ nm, $w = 140$ nm around 750 nm (black arrow in Fig. 6a). It suggests that the period of the nanowire array is able to tune the sign of the linear dichroism. The good linearity can be attributed to the distinct coupling of excitons with plasmons along the two orthogonal polarizations, leading to different degrees of enhancement of the PL in TE and TM directions.

For the direct bandgap transition, the maximal linearity is always observed in the nanowire array with $p = 600$ nm because this period is comparable with the emission wavelength $\lambda \sim 636$ nm thus satisfies the condition of the constructive interference $p \sim \lambda$, thereby leading to the most remarkable enhancement in the TE polarization direction among different periods of the nanowire array (red curves in Figure S3a,d). This is consistent with the highest transmittance of the TE polarized light in the forward direction among three types of periods of the nanowire array (red curves in Figure S4a,b,e,f). At the same time, the emission in the TM polarization direction is low (red curves in Figure S3b,e) because of the high reflectance in the backward direction (red curves in Figure S4c,d,g,h). Moreover, the wire width is a key parameter to tune the linearity of the PL emission of the direct bandgap transition since the dominating plasmon mode and the reflectance of the nanowire array have a close dependence on the wire width (Fig. 5). As a result, LD increases from 0.43 to 0.64 by increasing the wire width from 145 to 312 nm as shown in Fig. 6b.

To show intuitively the extraordinary polarization modulation through the anisotropic enhancement of the nanowire array, PL peaks as a function of the detection angle for indirect (red dots) and direct (blue dots) bandgap transitions are characterized for the pristine bilayer $WS_2$ and $WS_2$-Ag hybrid nanostructures with the periods of 400 and 600 nm as shown in Fig. 6c–e. For the indirect bandgap transition, PL is randomly polarized in the pristine $WS_2$ (Fig. 6c), then becomes linearly polarized in perpendicular (Fig. 6d) or parallel (Fig. 6e) to the long axis of the wire for $p = 400$ and 600 nm wire array respectively. For the direct bandgap transition, PL transforms from random to linear with the polarization fixed along the wire despite that the period of the wire array is different. In summary, large linearity is obtained for both indirect and direct bandgap transitions in bilayer $WS_2$. The former arises from the strong anisotropic enhancement of the PL in both TE and TM polarization directions

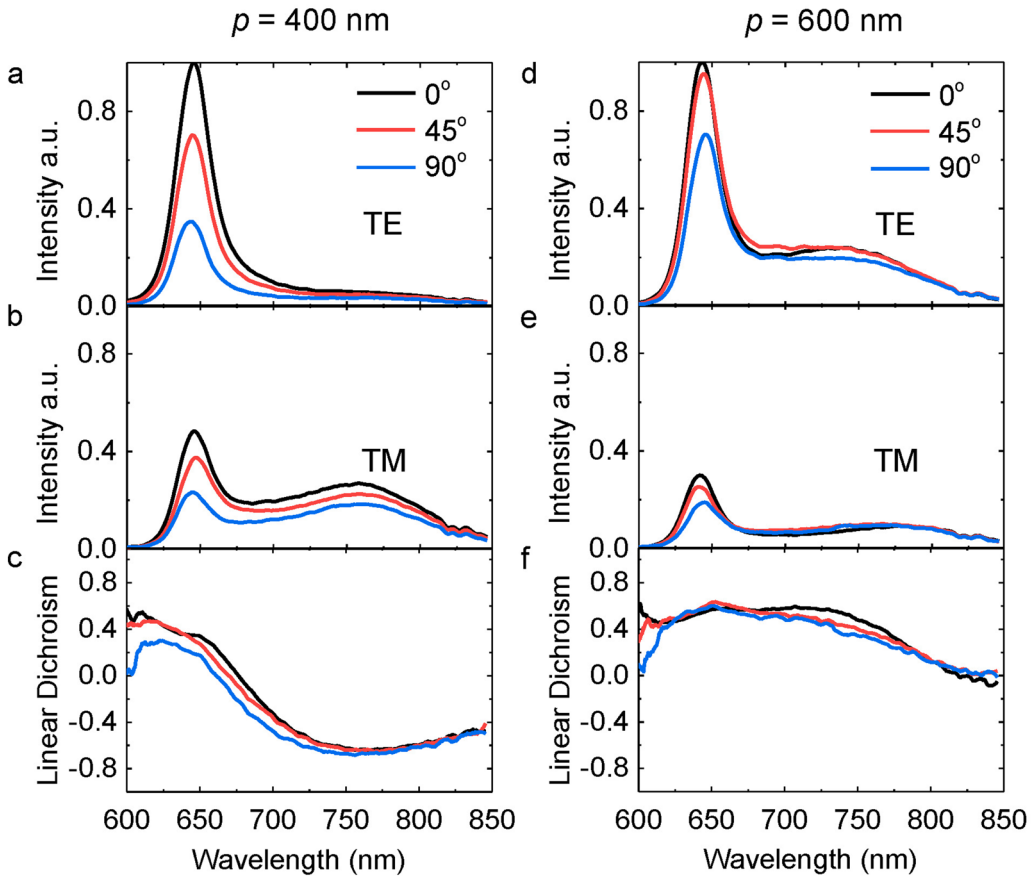


**Figure 7.** Anisotropic PL emission as a function of polarization angles of the laser excitation. Normalized intensity of the PL in the TE (**a**, **d**) and TM (**b**, **e**) polarization directions for the incident polarization angle at 0° (black curve), 45° (red curve), and 90° (blue curve), respectively. (**c**), (**f**) The corresponding linear dichroism. The periods of nanowire arrays in the hybrid $WS_2$-Ag nanostructures are 400 and 600 nm for the left and right columns, respectively.

dominated by either the plasmonic or waveguide mode of the metal wire array. The latter is attributed to the enhancement/suppression of the PL in the TE/TM polarization directions based on the enhanced transmission/reflection of the nanowire array in orthogonal polarizations.

*Anisotropic emission as a function of the polarization angle of the excitation.* In the above, the polarization of the incident laser is fixed along the wire. What will happen if we change the incident polarization direction? For the $WS_2$-Ag wire hybrid nanostructure with $p = 400$ nm, the normalized intensity of the PL in the TE/TM polarization direction is 1/0.48, 0.7/0.37 and 0.35/0.23 for the direct bandgap transition and 0.059/0.27, 0.050/0.23, 0.034/0.18 for the indirect bandgap transition when the incident polarization angle increases from 0°, 45° to 90° (Fig. 7a,b). It suggests that the intensity of the PL decreases when the incident polarization relative to the long axis of the wire is rotated from parallel (0°) to perpendicular (90°). This is probably due to the different excitation efficiency at different incident angles. The excitation is the strongest at 0° incidence due to the maximum absorption as manifested by the deeper reflection dip at ~ 532 nm as shown by the black curve in Fig. 3b. The absorption decreases with increasing the angle via 45° to 90° because the reflectance increases as manifested by the red curve in Fig. 3b resulting in the descending trend of the PL emission. Since both TE and TM polarizations decrease, the linear dichroism keeps almost the same at different excitation angles as shown in Fig. 7c.

For the hybrid nanostructure with $p = 600$ nm, a descending trend as a function of the incident polarization angle can also be observed in both TE and TM polarizations (Fig. 7d,e). But the difference of the PL intensity between 0° and 90° is smaller than that of the 400 nm period wire array (Fig. 7a,b) because the difference of the absorption at the excitation wavelength (532 nm) between TE and TM polarizations is smaller (Fig. 3d). The linear dichroism keeps almost the same for different incident polarization angles (Fig. 7f), suggesting that the degree of the linearity of the PL emission is determined by the geometry of the wire array rather than the polarization angle of the laser excitation.

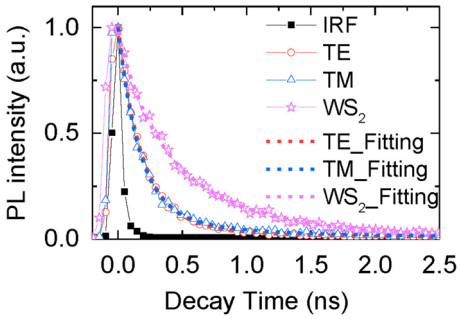


**Figure 8.** Time and polarization-resolved PL spectra of the bare $WS_2$ (pink star curve) and the hybrid nanostructure. PL lifetimes of the TE and TM polarizations of the hybrid nanostructure are indicated by the red dot (TE) and blue triangle (TM) curves. Data are fitted by two-component exponentials (dashed curves with the corresponding color).

| | t1 (ps) | t2 (ps) |
|---|---|---|
| Hybrid_TE | 174 ± 5 (88%) | 600 ± 80 (12%) |
| Hybrid_TM | 156 ± 5 (85%) | 593 ± 60 (15%) |
| $WS_2$ | 383 ± 30 (78%) | 1040 ± 230 (22%) |

**Table 1.** PL lifetime of $WS_2$ monolayer with/without the integration of the nanowire array ($p = 600$ nm, $w = 170$ nm). The lifetime and fractional amplitude[49] of each fitting component are displayed in the table.

## Discussion

Conventional optical modulators suffer from large volume, single function and passive modulation, thus are hard to be directly applied to photonic circuits. Here the highly confined metasurface-TMDCs hybrid systems provide a new route toward the emerging flat optics, where the intensity, polarization and wavelength of light can be tuned by tailoring the direction and magnitude of the plasmon-exciton coupling. Such a hybrid system is not limited to $WS_2$ samples. Take mode II as an example, it would be red shifted from 550 to 850 nm when the period of the nanowire array increases from 400 to 800 nm (Figure S5). The spectra cover almost the whole range of bandgaps of normal TMDC mono- and few layers, for instance, 620, 650, 750 and 800 nm for $WS_2$, $MoS_2$, $WSe_2$, $MoSe_2$ monolayers respectively. Hence, it is highly promising that various TMDCs with different optical bandgap transitions can be controlled by the plasmonic nanowire array.

It is noteworthy that mechanisms of the intensity enhancement and the anisotropy of the PL are different at different wavelengths. The exciton-plasmon coupling dominates the PL enhancement around 750 nm. Significant enhancements of the PL (7 folds in TM for the 400 nm period wire array and 4.2 folds in TE for the 600 nm period wire array) are attributed to the plasmonic modes I and II (Fig. 3), which provide localized and guided plasmonic fields, respectively, to increase the spontaneous emission rate of the PL in specific polarization directions. Hence, the anisotropy of the PL can be ascribed to the different degrees of enhancement between TE and TM polarizations. However, for the emission around 640 nm, we attribute the enhancement to both the coherent scattering of the nanowire array and the exciton-plasmon coupling. The enhancement in the TE polarization direction is moderate (less than 2 folds), as shown by the red curves in Fig. 4d–h. Because the emission wavelength is comparable to the period of the nanowire array thus the constructive interference takes place. Moreover, the plasmonic mode of the nanowire array (represented as the reflectance dip around 580 nm for the TE polarization in Fig. 3c,d) located on the blue side of the PL emission wavelength may contribute to the enhancement. We have found that the blue shift of this mode, as indicated by the dashed black arrow in Fig. 5e, coincides well with the descending trend of the PL intensity in the TE polarization direction upon increasing the wire width (Fig. 4d–h).

To provide more evidence of the exciton-plasmon coupling for the PL enhancement ~ 640 nm, time-resolved photoluminescence is measured to determine the PL decay time of $WS_2$ integrated with/without the nanowire array (Supplementary note 4). Silver nanowire array, with 600 nm in period and 170 nm in width, is patterned on monolayer $WS_2$ (Figure S6a). The polarization-resolved lifetimes of the excitonic emission for the $WS_2$-Ag wire hybrid nanostructure and the bare $WS_2$ are shown in Fig. 8. The hybrid structure exhibits a shorter lifetime than the bare $WS_2$. Specifically, the decay process is ~ 2 times faster when the $WS_2$ is integrated with the nanowire array (Table 1). Also, the decay time is quite similar between TE and TM for the hybrid nanostructure, which is probably due to the almost equal absorption for both polarizations (red and blue arrows in Figure S6b). The reduced lifetime can be explained as the plasmonic speed-up effect[48]. The plasmonic fields increase the recombination rate between electrons and holes in the $WS_2$, causing the increase of the spontaneous emission rate and hence the PL intensity. Similar decay time between TE and TM implies that the PL enhancement is effective to both polarizations. As a result, the anisotropy of the PL emission at 640 nm should be originated from the preferred

scattering direction of the nanowire array, *i.e*. TE polarization in the forward direction (Fig. 5a,c) and the TM polarization in the backward direction (Fig. 5b,d).

In brief, the linearity of the PL at 750 nm results from the polarization-dependent plasmonic coupling leading to different degrees of enhancement in TE and TM polarizations. In contrast, the linearity of the PL at 640 nm is attributed to the geometrical birefringence of the nanowire array, which is represented as a high transmission of the TE polarization in the forward direction and a high reflection of the TM polarization in the backward direction. This is different from the wire grid polarizer whose period is much smaller than the tailored wavelength of light in which the geometrical birefringence is characterized as a high transmission of the TM polarization in the forward direction and high reflection of the TE polarization in the backward direction.

## Conclusion

In conclusion, we have demonstrated the strong anisotropic enhancement of the PL emission in $WS_2$ integrated with the plasmonic nanowire array. The enhancement at different optical bandgap transitions stems from different mechanisms. For the indirect bandgap transition around 750 nm, multifold enhancement of the PL is attributed to the coupling of excitons with either the localized plasmon mode of metallic nanowires in the TM polarization direction or the plasmonic waveguide mode of the nanowire array on the dielectric substrate in the TE polarization direction. The localized mode I enables a higher degree of enhancement up to 7 because of a smaller mode volume and a stronger field localization around the surface of the metal wire. The waveguide mode II exhibits a spectral shift as a function of the period of the nanowire array allowing for the modulation of the excitonic emission in a wide spectral range. In contrast, for the direct bandgap transition, only a moderate enhancement of the PL (1–2.5x) in the TE polarization direction was observed which is probably due to the coherent superposition of the TE polarized light in the periodic array, just like the zero-order interference maximum in the diffraction grating. The linearity has a strong dependence on the wire width and periods of the array while it is less influenced by the polarization angle of the incident laser. Our study offers new opportunities for establishing ultrathin photonic devices with multi-functionalities which allows technical advancements in various important areas such as tunable displaying, ultrasensitive sensing, and encoded imaging.

## Data availability

*Scientific Reports* requires the inclusion of a data availability statement with all submitted manuscripts, as this journal requires authors to make available materials, data, and associated protocols to readers.

Received: 13 December 2020; Accepted: 5 April 2021
Published online: 12 May 2021

## References

1. Xia, F., Wang, H., Xiao, D., Dubey, M. & Ramasubramaniam, A. Two-dimensional material nanophotonics. *Nat. Photonics* **8**, 899–907 (2014).
2. Withers, F. *et al.* Light-emitting diodes by band-structure engineering in van der Waals heterostructures. *Nat. Mater.* **14**, 301–306 (2015).
3. Pu, J. & Takenobu, T. Monolayer transition metal dichalcogenides as light sources. *Adv. Mater.* **30**, 1707627 (2018).
4. Zhang, Y. J., Oka, T., Suzuki, R., Ye, J. T. & Iwasa, Y. Electrically switchable chiral light-emitting transistor. *Science* **344**, 725–728 (2014).
5. Tu, L., Cao, R., Wang, X. *et al.* Ultrasensitive negative capacitance phototransistors. *Nat. Commun.* **11**, 101 (2020).
6. Lee, H., Ahn, J., Im, S., Kim, J. & Choi, W. High-responsivity multilayer $MoSe_2$ phototransistors with fast response time. *Sci. Rep.* **8**, 11545 (2018).
7. Feng, J., Qian, X., Huang, C. W. & Li, J. Strain-engineered artificial atom as a broad-spectrum solar energy funnel. *Nat. Photonics* **6**, 866–872 (2012).
8. Sun, Z., Martinez, A. & Wang, F. Optical modulators with 2D layered materials. *Nat. Photonics* **10**, 227–238 (2016).
9. Li, B. *et al.* Single-nanoparticle plasmonic electro-optic modulator based on $MoS_2$ monolayers. *ACS Nano* **11**, 9720–9727 (2017).
10. Lu, J. M. *et al.* Evidence for two-dimensional Ising superconductivity in gated $MoS_2$. *Science* **350**, 1353–1357 (2015).
11. Liu, X. & Hersam, M. C. 2D materials for quantum information science. *Nat. Rev. Mater.* **4**, 669–684 (2019).
12. Han, C. & Ye, J. Polarized resonant emission of monolayer $WS_2$ coupled with plasmonic sawtooth nanoslit array. *Nat. Commun.* **11**, 713 (2020).
13. Subramanian, S., Kumar, K. & Dhawan, A. Palladium-coated narrow groove plasmonic nanogratings for highly sensitive hydrogen sensing. *RSC Adv.* **10**, 4137 (2020).
14. Tittl, A., Giessen, H. & Liu, N. Plasmonic gas and chemical sensing. *Nanophotonics* **3**, 157–180 (2014).
15. Cheng, F., Yang, X. & Gao, J. Ultrasensitive detection and characterization of molecules with infrared plasmonic metamaterials. *Sci. Rep.* **5**, 14327 (2015).
16. Bao, Y. *et al.* Coherent pixel design of metasurfaces for multidimensional optical control of multiple printing-image switching and encoding. *Adv. Funct. Mater.* **28**, 1805306 (2018).
17. Zhao, B. *et al.* A high-efficiency multispectral filter based on plasmonic hybridization between two cascaded ultrathin nanogratings. *Molecules* **24**, 2038 (2019).
18. Mei, Z. & Tang, L. Surface-plasmon-coupled fluorescence enhancement based on ordered gold nanorod array biochip for ultrasensitive DNA analysis. *Anal. Chem.* **89**, 633–639 (2017).
19. Schirato, A. *et al.* Transient optical symmetry breaking for ultrafast broadband dichroism in plasmonic metasurfaces. *Nat. Photonics* **14**, 723–727 (2020).
20. Feng, F., Si, G., Min, C., Yuan, X. & Somekh, M. On-chip plasmonic spin-hall nanograting for simultaneously detecting phase and polarization singularities. *Light Sci. Appl.* **9**, 95 (2020).
21. Dufferwiel, S. *et al.* Valley coherent exciton-polaritons in a monolayer semiconductor. *Nat. Commun.* **9**, 4797 (2018).
22. Chen, Y. J., Cain, J. D., Stanev, T. K., Dravid, V. P. & Stern, N. P. Valley-polarized exciton–polaritons in a monolayer semiconductor. *Nat. Photonics* **11**, 431–436 (2017).
23. Felici, M. *et al.* Broadband enhancement of light-matter interaction in photonic crystal cavities integrating site-controlled quantum dots. *Phys. Rev. B* **101**, 205403 (2020).

24. Dovzhenko, D. S., Ryabchuk, S. V., Rakovich, Y. P. & Nabiev, I. R. Light–matter interaction in the strong coupling regime: configurations, conditions, and applications. *Nanoscale* **10**, 3589–3605 (2018).
25. Butun, S., Tongay, S. & Aydin, K. Enhanced light emission from large-area monolayer $MoS_2$ using plasmonic nanodisc arrays. *Nano Lett.* **15**, 2700–2704 (2015).
26. Sortino, L. *et al.* Enhanced light-matter interaction in an atomically thin semiconductor coupled with dielectric nano-antennas. *Nat. Commun.* **10**, 5119 (2019).
27. Palacios, E., Park, S., Butun, S., Lauhon, L. & Aydin, K. Enhanced radiative emission from monolayer $MoS_2$ films using a single plasmonic dimer nanoantenna. *Appl. Phys. Lett.* **111**, 031101 (2017).
28. Mey, O. *et al.* Enhancement of the monolayer tungsten disulfide exciton photoluminescence with a two-dimensional material/air/gallium phosphide in-plane microcavity. *ACS Nano* **13**, 5259–5267 (2019).
29. Lee, B. *et al.* Fano resonance and spectrally modified photoluminescence enhancement in monolayer $MoS_2$ integrated with plasmonic nanoantenna array. *Nano Lett.* **15**, 3646–3653 (2015).
30. Kim, S. H. *et al.* Broadband surface plasmon lasing in one-dimensional metallic gratings on semiconductor. *Sci. Rep.* **7**, 7907 (2017).
31. Christ, A., Tikhodeev, S. G., Gippius, N. A., Kuhl, J. & Giessen, H. Waveguide-plasmon polaritons: strong coupling of photonic and electronic resonances in a metallic photonic crystal slab. *Phys. Rev. Lett.* **91**, 183901 (2003).
32. Porto, J. A., García-Vidal, F. J. & Pendry, J. B. Transmission resonances on metallic gratings with very narrow slits. *Phys. Rev. Lett.* **83**, 2845–2848 (1999).
33. Han, C., Parrott, E. P. J. & Pickwell-MacPherson, E. Tailoring metamaterial microstructures to realize broadband polarization modulation of terahertz waves. *IEEE J. Sel. Top. Quantum Electron.* **23**, 1–6 (2017).
34. Parrott, E. P. J. *et al.* Vanadium dioxide devices for terahertz wave modulation: a study of wire grid structures. *Nanotechnology* **27**, 205206 (2016).
35. Lobanov, S. V., Gippius, N. A., Tikhodeev, S. G. & Butov, L. V. Control of light polarization by voltage in excitonic metasurface devices. *Appl. Phys. Lett.* **111**, 241101 (2017).
36. Han, C., Parrott, E. P. J., Humbert, G., Crunteanu, A. & Pickwell-MacPherson, E. Broadband modulation of terahertz waves through electrically driven hybrid bowtie antenna-$VO_2$ devices. *Sci. Rep.* **7**, 12725 (2017).
37. Kosako, T., Kadoya, Y. & Hofmann, H. F. Directional control of light by a nano-optical Yagi-Uda antenna. *Nat. Photonics* **4**, 312–315 (2010).
38. Zhang, D. *et al.* Polarization properties of subwavelength metallic gratings in visible light band. *Appl. Phys. B* **85**, 139–143 (2006).
39. Yi, D., Yan, Y., Liu, H., Lu, S. & Jin, G. Broadband polarizing beam splitter based on the form birefringence of a subwavelength grating in the quasi-static domain. *Opt. Lett.* **29**, 754–756 (2004).
40. McCreary, A. *et al.* Distinct photoluminescence and Raman spectroscopy signatures for identifying highly crystalline $WS_2$ monolayers. *J. Mater. Res.* **31**, 931–944 (2016).
41. Zeng, H. *et al.* Optical signature of symmetry variations and spin-valley coupling in atomically thin tungsten dichalcogenides. *Sci. Rep.* **3**, 1608 (2013).
42. Wang, F. *et al.* Strain-induced phonon shifts in tungsten disulfide nanoplatelets and nanotubes. *2D Mater.* **4**, 015007 (2016).
43. Lundt, N. *et al.* Optical valley hall effect for highly valley-coherent exciton-polaritons in an atomically thin semiconductor. *Nat. Nanotechnol.* **14**, 770–775 (2019).
44. Ngo, Q. M., Hoang, T. T., Nguyen, D. L., Vu, D. L. & Pham, V. H. Metallic assisted guided-mode resonances in slab waveguide gratings for reduced optical switching intensity in bistable devices. *J. Opt.* **15**, 055503 (2013).
45. Chen, Y., Munechika, K. & Ginger, D. S. Dependence of fluorescence intensity on the spectral overlap between fluorophores and plasmon resonant single silver nanoparticles. *Nano Lett.* **7**, 690–696 (2007).
46. Bharadwaj, P. & Novotny, L. Spectral dependence of single molecule fluorescence enhancement. *Opt. Express* **15**, 14266–14274 (2017).
47. Wang, B., Liu, M., Huang, T. & Zhao, C. Micro/Nanostructures for far-field thermal emission control: an overview. *ES Energy Environ.* **6**, 18–38 (2019).
48. Bogdanov, S. I., Boltasseva, A. & Shalaev, V. M. Overcoming quantum decoherence with plasmonics. *Science* **364**, 532–533 (2019).
49. McCreary, K. M., Currie, M., Hanbicki, A. T., Chuang, H.-J. & Jonker, B. T. Understanding variations in circularly polarized photoluminescence in monolayer transition metal dichalcogenides. *ACS Nano* **11**, 7988–7994 (2017).


## Acknowledgements

This work was supported by CAS Pioneer Hundred Talents Program of China and European Research Council (consolidator Grant No. 648855 Ig-QPD).

## Author contributions

C.H. and J.Y. conceived the experiment(s). C.H. conducted the experiment(s) and simulation(s). C.H., Y.W. and W.Z. performed statistical analysis and figure generation. C.H., M.L. and J.Y. revised the manuscript. All authors reviewed the manuscript.

## Competing interests

The authors declare no competing interests.

## Additional information

**Supplementary information** The online version contains supplementary material available at https://doi.org/10.1038/s41598-021-89136-0.

**Correspondence** and requests for materials should be addressed to C.H. or J.Y.

**Reprints and permissions information** is available at www.nature.com/reprints.

**Publisher's note** Springer Nature remains neutral with regard to jurisdictional claims in published maps and institutional affiliations.